European Journal of Medicinal Chemistry 139 (2017) 482–491

Contents lists available at ScienceDirect

European Journal of Medicinal Chemistry

journal homepage: http://www.elsevier.com/locate/ejmech

Research paper

Crystal structure of *Porphyromonas gingivalis* dipeptidyl peptidase 4 and structure-activity relationships based on inhibitor profiling

Dean Rea [c], Roos Van Elzen [a, 1], Hans De Winter [b], Sebastiaan Van Goethem [b, 2], Bart Landuyt [d], Walter Luyten [d], Liliane Schoofs [d], Pieter Van Der Veken [b], Koen Augustyns [b], Ingrid De Meester [a], Vilmos Fülöp [c], Anne-Marie Lambeir [a, *]

[a] Laboratory of Medical Biochemistry, Department of Pharmaceutical Sciences, University of Antwerp, Universiteitsplein 1, B-2610 Antwerp, Belgium
[b] Laboratory of Medicinal Chemistry, Department of Pharmaceutical Sciences, University of Antwerp, Universiteitsplein 1, B-2610 Antwerp, Belgium
[c] School of Life Sciences, University of Warwick, Gibbet Hill Road, Coventry, CV4 7AL, UK
[d] Animal Physiology and Neurobiology Section, Department of Biology, KULeuven, Naamsestraat 59, B-3000 Leuven, Belgium

ARTICLE INFO

Article history:
Received 15 June 2017
Received in revised form
7 August 2017
Accepted 8 August 2017
Available online 10 August 2017

Keywords:
Dipeptidyl peptidase 4
Peptidase inhibitor
Porphyromonas gingivalis
Biofilm
Dipeptidyl peptidase 9

ABSTRACT

The Gram-negative anaerobe *Porphyromonas gingivalis* is associated with chronic periodontitis. Clinical isolates of *P. gingivalis* strains with high dipeptidyl peptidase 4 (DPP4) expression also had a high capacity for biofilm formation and were more infective. The X-ray crystal structure of *P. gingivalis* DPP4 was solved at 2.2 Å resolution. Despite a sequence identity of 32%, the overall structure of the dimer was conserved between *P. gingivalis* DPP4 and mammalian orthologues. The structures of the substrate binding sites were also conserved, except for the region called S2-extensive, which is exploited by specific human DPP4 inhibitors currently used as antidiabetic drugs. Screening of a collection of 450 compounds as inhibitors revealed a structure-activity relationship that mimics in part that of mammalian DPP9. The functional similarity between human and bacterial DPP4 was confirmed using 124 potential peptide substrates.

1. Introduction

Periodontal disease develops when bacteria of the dental plaque migrate from the dental root hard tissues to nearby soft tissues. This results in chronic inflammation leading to destruction of the periodontal ligament and the alveolar bone that supports the teeth. The process by which a generally benign biofilm transforms into pathological periodontitis is complex and remains poorly understood. However, the presence of one particular species, the Gram-negative anaerobe *Porphyromonas gingivalis*, is considered to be an indicator of progression of chronic periodontitis [1,2]. Periodontal disease, and specifically the presence of *P. gingivalis*, are risk factors for cardiovascular disease, aspiration pneumonia and low birth weight [3–5]. A wide array of virulence factors have been described for *P. gingivalis* that reflect the different processes by which the bacterium transforms from a commensal organism to a pathogen: biofilm formation, anaerobic growth, adhesion, suppression/activation of inflammatory responses, invasion, tissue degradation and intracellular survival in gingival epithelial cells and host immune cells (reviewed by Refs. [6,7]). *P. gingivalis* produces a unique set of proteases that are believed to be required for nutrient provision during its compulsory asaccharolytic growth, but may also contribute to evasion of the host immune system, adhesion and degradation of extracellular matrix [8–10]. One of these proteases is *P. gingivalis* dipeptidyl peptidase 4 (pgDPP4). The gene encoding pgDPP4 was first cloned and sequenced in 2000 [11], and the protein is secreted but remains associated with the membrane [12]. PgDPP4 is a proline-specific dipeptidyl peptidase that cleaves peptides related to immune responses and inflammation

Abbreviations: DPP, dipeptidyl peptidase; hDPP4, human dipeptidyl peptidase 4; MAD, Multiwavelength Anomalous Dispersion; pgDPP4, *Porphyromonas gingivalis* dipeptidyl peptidase 4; SAR, structure-activity relationship.

* Corresponding author.
E-mail addresses: Roos.VanElzen@histogenex.com (R. Van Elzen), hans.dewinter@uantwerpen.be (H. De Winter), sebastiaan.vangoethem@pfizer.com (S. Van Goethem), bart.landuyt@kuleuven.be (B. Landuyt), walter.luyten@kuleuven.be (W. Luyten), liliane.schoofs@kuleuven.be (L. Schoofs), pieter.vanderveken@uantwerpen.be (P. Van Der Veken), koen.augustyns@uantwerpen.be (K. Augustyns), ingrid.demeester@uantwerpen.be (I. De Meester), v.fulop@warwick.ac.uk (V. Fülöp), anne-marie.lambeir@uantwerpen.be (A.-M. Lambeir).
[1] Current address: Histogenex N.V. Lindendreef 1 B-2020 Antwerp Belgium.
[2] Current address: Pfizer Belgium, Rijksweg 12, B-2870 Puurs Belgium.

http://dx.doi.org/10.1016/j.ejmech.2017.08.024
0223-5234/

in vitro. Evidence suggests pgDPP4 interacts with extracellular matrix proteins such as fibronectin and collagen, thereby promoting collagen degradation by matrix metalloproteinases activated by the host inflammatory response [13,14]. Mice injected with a DPP4-deficient mutant strain developed fewer abscesses and survived longer than mice injected with the wild type (W83) strain [11], implicating pgDPP4 as a virulence factor. Transfection with recombinant pgDPP4 restored virulence, while a catalytically impaired DPP4 only partially restored the wild type phenotype [15]. Moreover, clinical isolates of *P. gingivalis* strains with high DPP4 expression had a higher capacity for biofilm formation and were more infective in a mouse abscess model [16].

pgDPP4 belongs to the same family of proteases (prolyl oligopeptidase family, S9 clanB, MEROPS database) as human DPP4 (hDPP4), with which it shares 32% amino acid sequence identity. This suggests a similar topology and enzymatic mechanism. Even though the catalytic residues and side chains forming the primary substrate-binding site are conserved, we noticed significant differences in the potency of selected inhibitors, and in the substrate specificity, between the bacterial and human enzymes [17]. Following preliminary crystallisation experiments [18], one of the aims of the present study was to identify the origins of these differences in the structure of pgDPP4, as a prerequisite to developing more specific inhibitors in the future. Both enzymes likely share substrates present in the oral cavity, the gingival epithelium and at sites of inflammation.

In humans, the inhibition of DPP4-catalyzed inactivation of incretins (intestinal peptides regulating insulin secretion) proved to be successful for the treatment of type 2 diabetes [19]. Over the last two decades, numerous DPP4 inhibitors have been synthesized, screened and tested for their antidiabetic activity, while other compounds have been prepared to address selectivity and to investigate the roles of several related peptidases. Thus, there exists a sizable collection of mammalian DPP family inhibitors available for screening against other targets. The collection used in the present work includes compounds that have been developed and characterized at the University of Antwerp during a long-standing research program on various peptidases, including DPP4, DPP2, DPP8, DPP9, fibroblast activating protein-α (FAP) and prolyl oligopeptidase (PREP). They are based on several chemical scaffolds [20–33]. The collection also includes reference compounds, such as the antidiabetic drugs sitagliptin, vildagliptin and linagliptin, and prototypical DPP2, DPP8/9 and FAP inhibitors. The aim of this study was to screen the collection of compounds present at the University of Antwerp. Additionally, an assortment of secreted peptides present at the University of Leuven was used as a substrate collection in order to investigate structure-function relationships in the active site of pgDPP4.

2. Results

2.1. Structural alignment of pgDPP4 and hDPP4

The overall structural similarity between both DPP4s is shown in Fig. 1. A sequence alignment with species-specific numbering is shown in the supplementary material.

Fig. 2 depicts the catalytic residues of pgDPP4 positioned in the electron density map. The active sites of pgDPP4 and hDPP4 are evidently similar. Direct transfer of the coordinates of the hDPP4 structures with different ligands into the active site of the aligned pgDPP4 structure (*i.e.* docking of ligands in pgDPP4 active site) reveals similar substrate binding pockets for both DPP4 enzymes. Table S1 in the supplementary material provides a list of all hDPP4 structures used in this work, together with references to the Protein Structure Database (PDB) and the original publications.

A narrow but deep S1-pocket is located next to the catalytic Ser-593 (adopting pgDPP4 numbering), and direct mapping of the many co-crystallized ligands from the human structures into the pgDPP4 structure reveals that this pocket could potentially accommodate a proline-moiety like the pyrrolidine ring of the Val-

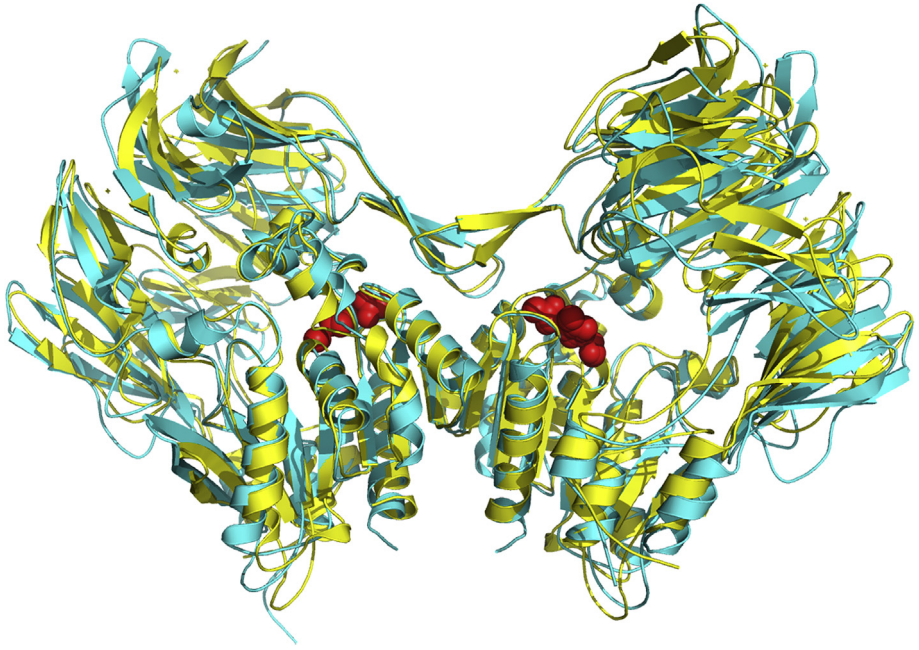

Fig. 1. Overall structural alignment of pgDPP4 and hDPP4.
Superposition of the crystal structures of human (cyan) and *P. gingivalis* (yellow) DPP4. The structure of the human form was taken from Grimshaw and coworkers (PDB ID 5KBY) [63]. Both structures are composed of two homodimers that are related by a two-fold axis. The catalytic triad residues in both structures are indicated with solid red spheres. Root-mean-squared deviation between the Cα atoms of both structures is 1.0 Å, indicating an extremely high level of structural similarity between the two proteins. (For interpretation of the references to colour in this figure legend, the reader is referred to the web version of this article.)

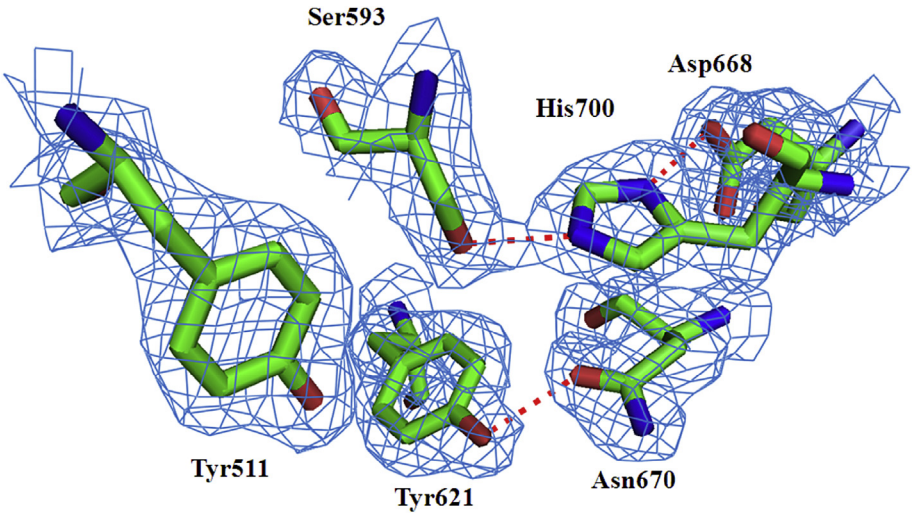

Fig. 2. The active site of pgDPP4.
Ser-593, His-700 and Asp-668 make up the catalytic triad. Tyr-511 is part of the oxyanion binding site, Tyr-625 and Asn-670 are part of the non-specific peptide/inhibitor binding sites. Important hydrogen bonds are shown as dotted lines. The SIGMAA [64] weighted 2mFo-ΔFc electron density is contoured at the 1.0 σ level, where σ represents the RMS electron density for the unit cell. Contours more than 1.4 Å from any of the displayed atoms have been removed for clarity.

pyrrolidide or a phenyl or halogen-substituted phenyl of many other ligands, including vildagliptin and sitagliptin (Table S1). The residues flanking the S1-pocket are identical in the human and *P. gingivalis* enzymes. The S1-pocket is hydrophobic; lipophilic residues Tyr-594, Tyr-625, Tyr-629, Trp-622 and Val-619 are located within 4 Å of the pyrrolidine ring of the co-crystallized Val-pyrrolidide ligand from the human structure (PDB ID 1N1M) A visual representation of the S1 pocket can be found in Fig. 4 of the paper by Rasmussen et al., 2002 [34].

In both DPP4 enzymes, the positive charge of the amino terminus of the substrate peptide is neutralized by the negative charges from two glutamate residues flanking the S2-pocket, namely Glu-195 and Glu-196. The location of both residues is identical in the two enzymes. Almost all analyzed ligands from the human DPP4 crystals contain a functionality that mimics the interaction with the two S2-flanking glutamates through a primary or secondary amine. The only exception is the diisopropyl fluorophosphate ligand (DFP) from the 1TKR crystal structure, since this ligand does not occupy the S2-pocket at all. Also noteworthy is the binding mode of compound 5AP (Pdb: 1RWQ, Table S1), since in addition to the normal interaction of the glutamates with the benzylamino group of 5AP, an additional hydrogen bond is formed between the aniline on the pyrimidine moiety and the backbone carbonyl of Glu-195.

Many of the co-crystallized ligands in hDPP4 bind well beyond the S2-pocket in a subsite labeled as “S2-extensive”. According to structural analysis performed by Nabeno and coworkers, this pocket is not defined in other related proline specific peptidases such as DPP8, DPP9 and FAP [35]. In hDPP4, the S2-extensive pocket is flanked by residues Val-207, Ser-209, Phe-357 and Arg-358 (hDPP4 numbering). Based on the structural alignment, these residues are not completely conserved in pgDPP4. Val-207 corresponds to Phe-197 in pgDPP4, the human Ser-209 corresponds to Gly-198 of pgDPP4 (with a deletion of the human Phe-208 for which there is no matching residue in pgDPP4), Arg-358 corresponds to Asp-329 in pgDPP4, and the human Phe-357 has no clear equivalent in pgDPP4 which makes the human S2-extensive pocket somewhat smaller (Fig. 3).

The amino acid differences between the human and *P. gingivalis* S2-extensive pocket presumably have implications for the design of selective drugs. It could be argued that ligands that take advantage of these local differences of the S2-extensive pocket might be more selective for a particular DPP4 form. A number of hDPP4 inhibitors have been described that interact with Phe-357 and Arg-358 of the human enzyme. These residues are located along the same side of the pocket. For example, compound S14 (Pdb: 2FJP) forms a hydrogen bond with Arg-358 and also forms a pi-stacking interaction with the phenyl ring of Phe-357. Additionally, both sitagliptin and teneligliptin undergo pi-stacking interactions with the side chain of Phe-357 (Fig. 3).

On the other side of the S2-extensive pocket, where Val-207 and Ser-209 are located in the human form, there are less opportunities for the design of more selective inhibitors since none of the co-crystallized examples in hDPP4 interact with either of these two residues.

2.2. Screening of the inhibitor collection

A collection of 450 compounds was screened, including clinically used DPP4 inhibitors and some reference compounds, shown in Scheme 1 and Table 1. Most of the compounds were dipeptide derivatives. Of these, 81 exhibited more than 50% inhibition at a concentration of 100 μM, and 33 displayed greater than 50% inhibition at 10 μM. As a rule, IC_{50} values were only determined for compounds that gave more than 50% inhibition at 10 μM. For these compounds, IC_{50} values ranged between 10 and 0.05 μM (supplementary material, Table S2). Compounds with a protected amino terminus, targeting PREP and FAP [22,23,25,30], showed no inhibition, confirming that pgDPP4 is a true dipeptidyl peptidase. Compounds with an isoindoline derivative in the P1 position (which confers selectivity towards DPP8/9) [33] in general did not appreciably inhibit pgDPP4, and neither did compounds with a phosphonate moiety attached to P1 (irreversible DPP inhibitors) [31]. The remaining compounds were assigned to one of two classes, based on their structural scaffold. Class 1 contains compounds with a variation of amino acids in P2 in combination with pyrrolidine or variations thereon in P1. Class 2 compounds have a variation in P2, not limited to natural amino acids, and have combinations of substitutions on the pyrrolidine ring.

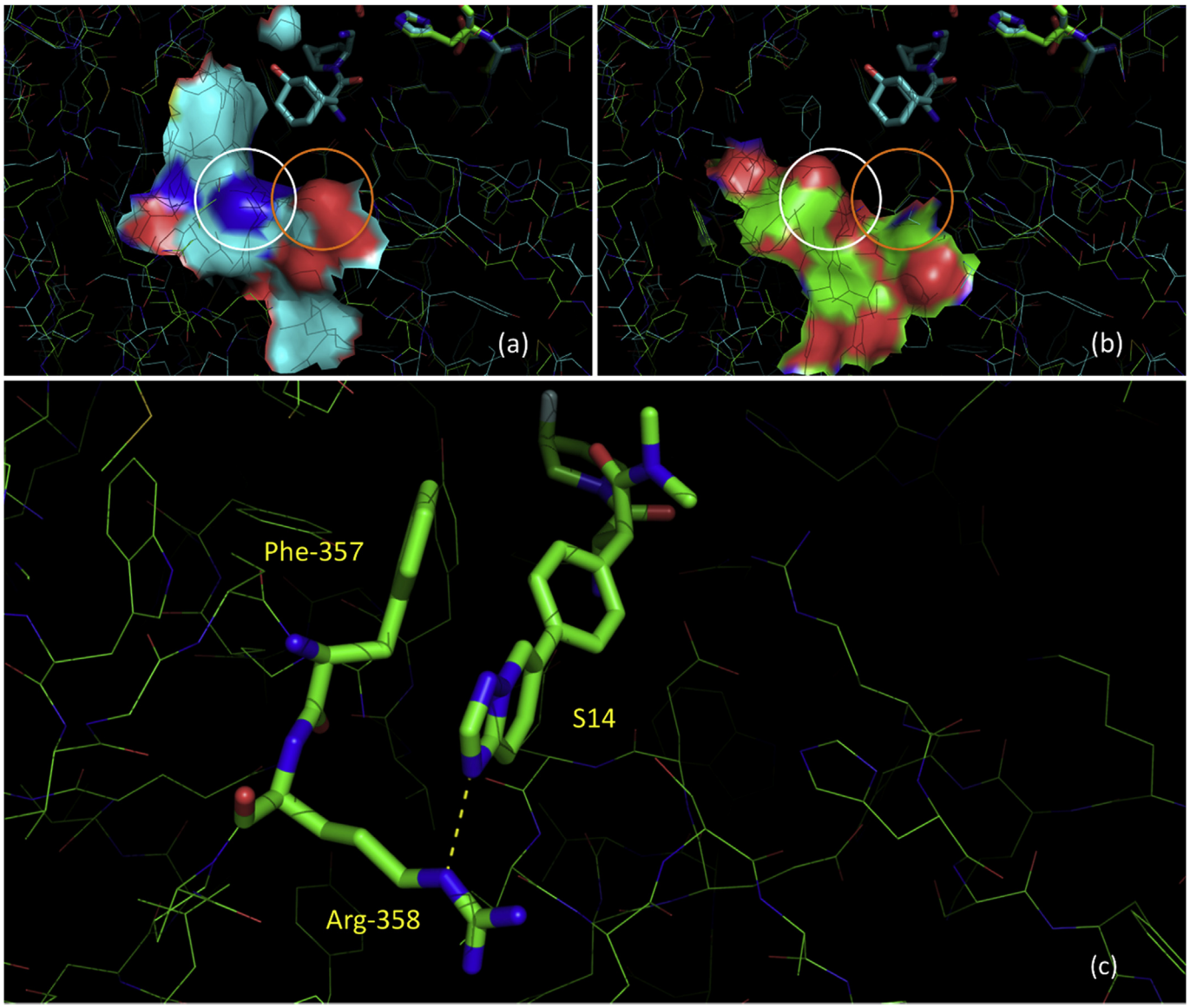

Fig. 3. The S2 extensive pocket.
(a) Overlay of the structures of pgDPP4 (green, without ligand) and hDPP4 (cyan, with ligand), highlighting the differences in shape and charge of the 'S2-extensive' pocket. Shown is the adamantyl sidechain of saxagliptin (PDB ID 3BJM) [36] and the surface (cyan, with positive and negative charges in blue and red, respectively) of hDPP4 as composed by residues Val-207, Ser-209, Phe-357 and Arg-358 (human numbering). The surface from Arg-358 is encircled in white and the surface from Ser-209 is encircled in orange. (b) Same view but now showing the surface (green, with positive and negative charges in blue and red, respectively) of the equivalent area of pgDPP4. The surface from Asp-329 is encircled in white and the surface from Gly-198 is encircled in orange (pgDPP4 numbering). (c) Crystal structure 2FJP [65] of hDPP4 showing compound S14 hydrogen-bonded to Arg-358. Also shown are Phe-357 and the potential pi-stacking interaction with the phenyl ring of the S14 ligand.

2.3. Structure-activity relationships (SAR) of inhibitors: S1 and S2 binding sites

Class 1 contains compounds that are based on Xaa-pyrrolidide, where Xaa is a variety of amino acids, and compounds that contain variable motifs replacing the pyrrole ring with Xaa = Ile, *allo*-Ile, Lys, *Z*-Lys or cyclohexylalanine. A preliminary study already demonstrated differences between pgDPP4 and human DPP4 [17], and the results of this small-scale study were reproduced and extended in the present work. Inhibition of pgDPP4 by Xaa-pyrrolidides was ordered: Val ≈ Ile ≈ *allo*-Ile ≈ Lys ≈ *Z*-Lys ≈ Thr, *Z*-Orn, Arg, *ZZ*-Arg, norLeu > Pro > Tyr > Ala > Cha, Phe, Trp, Cys, Orn, Glu, Gly. This is similar to hDPP4, except for lysine and threonine, which are more preferred by pgDPP4. By comparison, *allo*-Ile, *Z*-Lys and Lys are present in the P2 position of the strongest inhibitors of DPP9, and *ZZ*-Arg, His, Arg, *Z*-Orn, *Z*-lys, Orn and Lys pyrrolidides are all very good inhibitors for DPP2. Although Thr is not the best P2 residue for pgDPP4, it is the most effective for separating it from hDPP4, DPP9 and DPP2. The IC_{50} of Tyr-pyrrolidide was between 10 and 100 μM. Notably, a P2 proline is accepted less well by pgDPP4 than by hDPP4.

Still in class 1, it was found that at the P1 position the five-membered pyrrolidide ring is optimal for both DPP4s but the slightly larger piperidine provides some selectivity for pgDPP4. Ile-4-hydroxy-pyrrolidide was present in the inhibitor library but its affinity for pgDPP4 (and hDPP4) is at least 10-fold lower than Ile-pyrrolidide. Larger structures in P1 lead to loss of affinity. Iso-indoline, which conveys selectivity for DPP8/9, generally gives poor inhibition of pgDPP4. Some substituents on the pyrrolidide ring increase the affinity for the pgDPP4 active site. It has been known

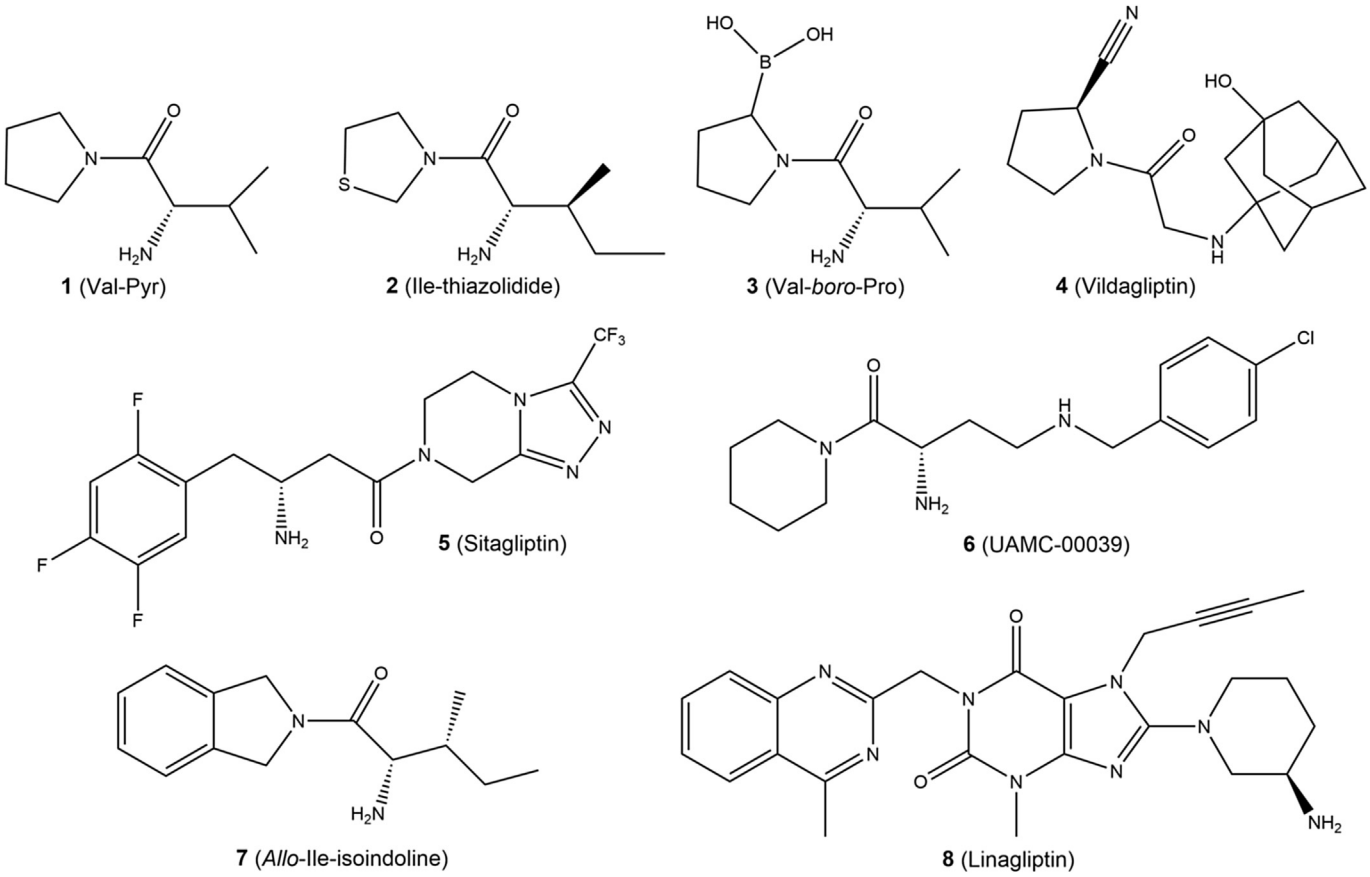

Scheme 1. Structures of the reference compounds listed in Table 1.

Table 1
Potency and selectivity of reference compounds.

Cpd	IC_{50} (μM)					Ref
	PgDPP4	DPP4	DPP8	DPP9	DPP2	
1	29 ± 1	5.4 ± 0.3	5.2 ± 0.3	11.3 ± 0.48	153 ± 12	[29]
2	19 ± 2	1.7 ± 0.1	6.0 ± 3.7	6.6 ± 0.4	28 ± 9	[29]
3	0.14 ± 0.01	0.022 ± 0.001	0.051 ± 0.002	Not reported	0.086 ± 0.007	[58]
4	1.3 ± 0.2	0.12 ± 0.01[a]	9.0 ± 0.1	0.68 ± 0.02	>1000	[35]
5	18 ± 1	0.04 ± 0.001	>50	>100	>100	[59]
6	>100	165 ± 9	142 ± 27	76.6 ± 6.1	<0.0005	[27]
7	10–100	90 ± 4	0.12 ± 0.01	0.29 ± 0.02	29 ± 1	[60]
8	10–100	0.002 ± 0.0002	>100	>100	>100	[61]

[a] Vildagliptin (4) is a slow-binding inhibitor with a K_i of 17 nM [38], its potency is underestimated by the IC_{50} value which was determined with a 15 min pre-incubation.

for some time that electrophiles such as a nitrile group on C2 can ameliorate the IC_{50} for all DPPs [29]. This is also the case for pgDPP4. The combination of an azide group at position 3 improves binding to pgDPP4 more than to hDPP4, but the resulting compounds still have a low selectivity.

Class 2 includes 2-cyano,4-azido-pyrrolidides with Leu, *allo*-Ile, Lys and Glu or Asp derivatives at the P2 position. In this class, the most selective pgDPP4 inhibitors were Lys-3-azo-2-cyano-pyrrolidide and N-2-naphtyl-Lys-4-azo-2-cyano-pyrrolidide, which were seven-fold more active against pgDPP4 than hDPP4. Large substituents on the Lys side chain appear to be easily accommodated, a property shared with human DPP2 and DPP8/9. When polar groups are introduced in the P2 side chain in a series of substituted Asp or Glu derivatives, there is a strict selectivity for a two-carbon spacer between the Cα and the carbonyl carbon atom. The resulting SAR is given in Table 2, and Fig. 4 displays the selectivity of the most potent compounds towards hDPP4 and DPP9. By analogy with hDPP4, one assumes that the compounds lacking the carbonitrile warhead are fast, reversible inhibitors. The kinetics of binding of vildagliptin and compounds **16**, **17** and **18** were monitored, but in all cases maximal inhibition was observed immediately after mixing and remained constant for 1 h.

2.4. SAR in the S′ substrate binding sites

Most of the compounds screened vary in the P1 and P2 positions. Interactions with the S′ substrate binding sites were not considered. There is one structure of hDPP4 (Pdb: 1NU8) that contains the inhibitor/substrate Ile-Pro-Ile. In this structure, the C-terminal Ile side chain is accommodated in the S1′ site. Reasoning

Table 2
IC_{50} values and selectivity of representative inhibitors.

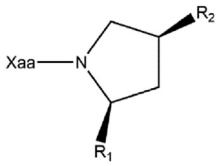

Compound	Xaa	R1	R2	IC_{50} (μM)	S.I.[a]	Ref[c]
9	*Z*-Lys	H	H	22 ± 3[b]	0.7	[29]
10	Lys	CN	H	1.6 ± 0.1	0.2	[29]
11	*Z*-Lys	CN	H	1.5 ± 0.1	0.02	[29]
12	2-amino-ethyl-Glu	CN	N_3	0.8 ± 0.6	0.5	[21]
13	piperazine-Glu	CN	N_3	0.48 ± 0.04	1.2	[21]
14	Lys	CN	N_3	0.33 ± 0.01	6.7	[29]
15	Ile	CN	N_3	0.31 ± 0.03	1.1	[29]
16	*Z*-Lys	CN	N_3	0.30 ± 0.02	1.8	[29]
17	*allo*-Ile	CN	N_3	0.23 ± 0.01	1.3	[29]
18	2-naphtyl-Lys	CN	N_3	0.079 ± 0.006	7.1	[29]

[a] Selectivity index = IC_{50} hDPP4/IC_{50} pgDPP4.
[b] Standard error on the fit.
[c] Original reference for IC_{50} values with hDPP4.

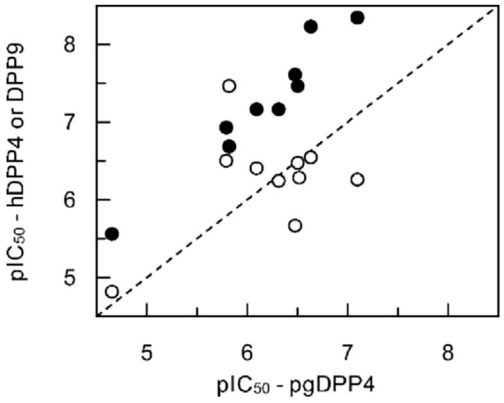

Fig. 4. Selectivity of the most potent compounds of the screening.
The pIC_{50} of hDPP4 (○) and DPP9 (●) is plotted versus the pIC_{50} of pgDPP4. Over an affinity range of more than two orders of magnitude, the IC_{50} of the inhibitors for DPP9 follow that of pgDPP4 whereas there is no corresponding increase in potency for hDPP4. Symbols above the diagonal (dotted line) indicate that the compound is more selective for the other enzyme than for pgDPP4.

that the extended substrate recognition site may reach further than the S1′ site, we investigated the substrate specificity of pgDPP4 and hDPP4 with a collection of 123 peptides (4–25 amino acids long) containing an N-terminal Xaa-Pro/Ala/Ser/Gly sequence (in almost equal proportion). In the conditions tested, 23 of these were cleaved by hDPP4 and 32 were hydrolyzed by pgDPP4. Pro and Ala in the P1 position determine the substrate specificity. None of the Xaa-Ser-containing peptides were cleaved, and only one Xaa-Gly peptide was processed. Peptides with a Xaa-Pro-Pro or Xaa-Ala-Pro motif were not cleaved either. The observed differences in the number of peptides cleaved, along with the frequency plots, indicate subtle differences between the DPP4s. pgDPP4-cleaved peptides have a higher frequency of aliphatic/hydrophobic side chains (V, F, L) in the P1′ position than the average peptide in the collection. Eleven peptides were cleaved by pgDPP4 but not by the human orthologue. Of these, five peptides had a penultimate proline and six contained one or two prolines in the P2′ to P4′ region. The P2-P2′ sequences of the peptides cleaved by pgDPP4 were used to construct a selectivity matrix (Table 3).

Table 3
Substrate specificity matrix of pgDPP4.

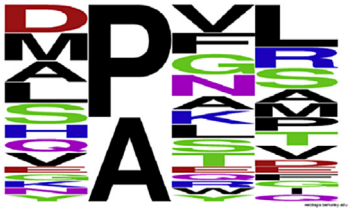

Amino acid	P2	P1	P1′	P2′
Gly	1/5[a]	1/21	2/8	1/4
Pro		15/28	0/4	2/7
Ala	3/5	12/31	2/4	2/4
Val	2/2		3/5	2/4
Leu	3/5		3/5	5/6
Ile	0/1			
Met	3/5			2/3
Phe	0/1		4/6	1/1
Tyr	2/2		1/1	
Trp	0/1		1/2	
Ser	3/7	0/25	2/3	3/6
Thr	0/2		2/4	2/4
Cys				0/2
Asn	1/1		3/4	0/2
Gln	3/4		1/2	1/2
Asp	3/8		0/1	1/3
Glu	1/3		1/2	1/4
Lys	1/4		2/4	1/2
Arg	0/1		1/3	4/4
His	2/3		0/2	0/2

[a] The frequency of cleavage is given by the ratio i/n with i the number of times the amino acid appears at the given position in a cleaved peptide and n the number of times the amino acid is present at the given position in the collection (sum of cleaved and uncleaved peptides). Xaa-Ser-containing and Xaa-Gly-containing peptides were not included in the specificity matrix and logo. Only unique P2-P2′ sequences were considered. Peptides with a blocked N-terminus were not included. The distribution logo was made using http://weblogo.berkeley.edu.

3. Discussion

The new crystal structure of pgDPP4 provides experimental evidence that, despite the low sequence identity, this bacterial enzyme has the same overall structure and catalytic mechanism as the human othologue. All key features of the catalytic machinery are structurally conserved, including the S1 pocket accommodating the proline, the catalytic triad, the oxy-anion hole required for stabilisation of the transition state and tetrahedral intermediates, the two glutamates that bind the positively charged N-terminus of the substrate and the S1′ pocket that maintains a sharp bend in the substrate's backbone. All these features have been described in the hDPP4 literature [34–36]. This structural conservation is also reflected in the fact that, with a few exceptions, both enzymes cleave the same substrates in a biologically relevant peptide collection (Table 3). However, there are local differences in areas that are not within reach of the side chains of the natural substrates but are occupied by synthetic inhibitors of hDPP4, notably the S2-extensive pocket (Fig. 3). Even though it was not possible to obtain ligand-bound structures under the specific crystallisation conditions, the pgDPP4 structure proved instrumental in understanding the specificity of inhibitors and may be usefull in future drug development projects targetting other proline specific dipeptidyl peptidases.

The conservation of the catalytic machinery provides an explanation for the increase in potency when a reactive group, a “warhead”, is present on the P1 of the inhibitors. In Table 2 and

Fig. 4, one observes a 10-fold increase in potency when a carbonitrile group is placed on the C2 of the pyrrolidide ring. The nitrile group is considered to sit in the active site as a transition state analog where the oxyanion hole provides stabilisation of a negative charge on the nitrogen, thus activating the carbon atom for a nucleophilic attack by the active site serine. This significantly enhances binding compared to compounds that lack the warhead but are otherwise the same. For hDPP4 and PREP, this has been observed on numerous occasions since the first reports in the 1990's [37]. This type of inhibitor is often called covalent, because in the crystal structures there is a short contact between the carbonitrile carbon atom and the oxygen of the side chain of the catalytic serine. From enzyme kinetics one cannot deduce whether these compounds form a covalent bond, since they behave as reversible competitive inhibitors. Very potent compounds sometimes display slow-binding and hyperbolic kinetics [38,39]. However, since the pgDPP4 structure has no ligand, and inhibition was essentially instantaneous, it remains unknown whether a covalent interaction occurs between the catalytic serine and the carbonitrile-containing compounds of this study. Assuming that all the compounds are reversible competitive inhibitors, and considering that the IC_{50} values were determined at a substrate concentration equal to the K_m, the IC_{50} values are a measure of the inhibition constants (K_i), allowing direct comparison of the potency between the different enzymes.

The pgDPP4 pharmacophore that emerged from the screening is shown in Fig. 5. In P1 a pyrrolidine is preferred, but in combination with certain P2 components, isoindoline and pyridine are accepted (for example **43**, **83**, **84** and **64** in Table S2) [17]. This is not the case for hDPP4, so it may be concluded that the S1 pocket of pgDPP4 is slightly larger than that of hDPP4, but not as large as that of DPP9 which prefers an isoindoline [33]. The carbonitrile warhead improves potency, but this is not specific for pgDPP4 because it is also observed with hDPP4, DPP9, DPP8 and DPP2 [29]. It requires *(S)* stereochemistry, like the peptide backbone of the natural substrates. A boronic acid in this position also improves potency (but not selectivity, **3** Table 1) and contrary to hDPP4 and DPP8, diphenyl phosphonates are ineffective [17,31], a phenomenon that is difficult to rationalise from the structure. The introduction of an azide group on the C4 affords a specific effect that is absent with hDPP4 but present with DPP9. Consequently, compounds **13**–**17** have a higher potency for pgDPP4 than for hDPP4, but the selectivity towards DPP9 does not change much. In Fig. 4, the line representing DPP9 inhibition is more or less parallel with the diagonal, indicating that the contribution of the azide substituent is independent from the P2 component. The azide substituent has to be in *cis* relative to the carbonitrile (**17** in Table 2 and 46 in Table S2). In previous studies, inhibitors were optimized for binding to DPP9 [21,29,30,32]. The results of the screening show an overlap between the pharmacophores of pgDPP4 and DPP9 with respect to the azide and the P2 component. The best P2 residues are large, often with a nitrogen atom on a carbon spacer and substituted with bulky or aromatic groups (**16**, **18** in Table 2 and 69, **72**, **73** in Table S2). The most likely explanation is that they bind specifically in the S2-extensive pocket, which is deeper in pfDPP4 than in hDPP4 and has a different charge distribution (Fig. 3). Since there is only a homology model but no crystal structure of DPP9 in the public domain, the results strongly suggest that the S2-extensive binding site could be targeted with likely success in DPP9 (and DPP8) [40]. DPP9 inhibitors are currently used to investigate a potential role of DPP9 in inflammation, but it is too soon to predict a clinical use [41,42].

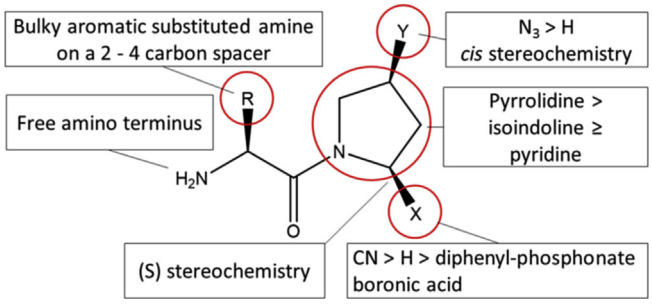

Fig. 5. Optimal pharmacophore for pgDPP4. The features influencing the pgDPP4 specificity over hDPP4 are circled in red. (For interpretation of the references to colour in this figure legend, the reader is referred to the web version of this article.)

By including a peptide collection, this study addressed the potential of the S′ binding sites for selectivity. However, from the crystal structure, there appears little evidence that enzyme-substrate interactions occur beyond the S2′ site. The observed differences between hDPP4 and pgDPP4 probably derive from structural properties of proline-containing peptides. Knowledge of the catalytic potency of serine proteases relies largely on historical studies with chymotrypsin and related proteases. How the different S9 family members deal with the intricacies of the chemistry required to cleave a post-proline bond therefore deserves further investigation [39].

In this study, we compared *P. gingivalis* DPP4 with human DPP4, and the results may be extrapolated to other bacterial DPP4s. The structure of at least one other bacterial DPP4 has been studied, namely the homologue from *Stenotrophomonas maltophilia*, which has the ability to hydrolyse peptide bonds following 4-hydroxyproline, as are found in collagen (PDB ID 2ECF) [43]. As our knowledge of bacterial genomes is rapidly expanding, it is very likely that other bacterial DPP4s will be discovered [44], and it may be interesting to verify whether they bind to the compounds currently used as antidiabetics. Although it is not completely clear at the moment how bacterial DPPs could be exploited as targets, this work at least offers a starting point for the development of specific compounds for bacterial enzymes; or a secondary use for existing drugs in the future.

4. Conclusion

Concluding, hDPP4 and pgDPP4 have a very similar overall structure and substrate specificity. Nevertheless, screening of the available inhibitor collection and docking of compounds in the pgDPP4 active site revealed that the clinically used DPP4 inhibitors have little affinity for pgDPP4. On the other hand, there is a certain overlap between the pgDPP4 and DPP9 pharmacophores. The crystal structure of pgDPP4 provides a starting point for the optimisation of inhibitors in the future, and for an increased understanding of inhibitor selectivity for proline-specific peptidases in general.

5. Experimental section

5.1. Materials

Gly-Pro-*p*-nitroanilide was purchased from Sigma (Diegem, Belgium). Inhibitor synthesis was described in the original publications [20–33]. Synthetic peptides were acquired from Thermo Scientific.

Cloning, expression and purification of recombinant pgDPP4 were performed as previously described [18].

5.2. Activity and inhibition measurements

Initial rates were determined by monitoring the release of *p*-nitroaniline at 405 nm using a Versamax (Molecular Devices, Sunnyvale CA, USA) microtitre plate reader at 37 °C. The molar absorptivity of *p*-nitroanilide is 10,200 $M^{-1}cm^{-1}$ and the path length was 0.58 cm. The reaction volume was 200 μl and contained ~0.2 mU of pgDPP4 and 0.25 mM Gly-Pro-*p*-nitroanilide in 50 mM TRIS-buffer, pH 8.3 containing 5% DMSO. Inhibitor stock solutions (100 mM) were made and diluted to 20× the final concentration in DMSO. Inhibitors were screened at a final concentration of 100 μM and 10 μM. For inhibitors with more than 50% inhibition at 10 μM, IC_{50} values were determined using 6–10 different inhibitor concentrations yielding between 90% and 10% inhibition. All measurements were performed in duplicate. IC_{50} values were calculated by fitting the data with the 4-parameter logistics equation using Grafit v5.

Assays for human DPP4 and bovine DPP9 were performed as described previously [29].

5.3. Enzyme-catalyzed peptide hydrolysis

The University of Leuven collection of putative neuropeptides and endocrine peptides was based on a combination of experimental peptidomics studies and bioinformatics [45,46]. Peptides with a penultimate Pro, Ala, Gly or Ser were chosen for this study. Peptides were incubated at a final concentration of 15 μM with 50 U/L DPP4 in 50 mM ammonium bicarbonate for 1 h at 37 °C. The reaction was stopped by addition of 0.1% trifluoroacetic acid. The mixture was spotted on a MALDI plate, left to dry and spotted with 5 mg/mL α-cyano-4-hydroxycinnamic acid matrix (Sigma, Diegem, Belgium) in 0.1%:50% trifluoroacetic acid:acetonitrile. Spectra were recorded with a MALDI TOF/TOF analyzer 4800 plus (Applied Biosystems, Foster City, CA, USA) in positive reflector mode over a mass range of 800–3500 or 300–2000 Da, depending on the size of the peptides.

5.4. Crystallisation, structure determination, model building and refinement

Recombinant pgDPP4 was crystallized as previously described [18] using the hanging-drop vapour-diffusion technique in 40% 2-methyl-2,4-pentanediol and 100 mM TRIS-HCl pH 8.0. Despite pgDPP4 sharing only 32% sequence identity with the porcine and human enzymes, partial molecular replacement was successful using the structures of these enzymes as search models. Diffraction data were therefore collected from selenomethionine-derived PgDPP4 crystals for structure determination by Multiwavelength Anomalous Dispersion (MAD). Crystals were removed from the crystallisation drop using a nylon loop, transferred directly to liquid nitrogen, and stored until needed. X-ray diffraction data to a resolution of 2.7 Å were collected from selenomethionine-derived crystals at peak, inflection point and remote wavelengths on beam line ID14-4 at the ESRF, Grenoble, following a fluorescence scan. All data were indexed, integrated and scaled with the HKL package [47]. Following anomalous Fourier synthesis from the molecular replacement partial solution using Phaser [48], the program SOLVE [49] successfully found 21 of the 25 selenium sites present in each of the eight subunits. After automatic model building using RESOLVE [49] and density modification with BUCCANEER [50], it was clear that some parts of some subunits were largely disordered. We therefore abandoned this attempt at structure solution and pursued a different crystal form. New crystallisation screens were set up with a fresh batch of protein and crystals were successfully grown in condition H10 of the MORPHEUS crystallisation screen [51] in a solution containing 10% (w/v) PEG 8000, 20% (v/v) ethylene glycol, 0.02 M sodium L-glutamate, 0.02 M DL-alanine, 0.02 M glycine, 0.02 M DL-lysine, 0.02 M DL-serine, and 0.1 M BICINE/TRIS pH 8.5. The new crystal form diffracted X-rays to 2.2 Å resolution at our in-house X-ray source, and crystals belonged to the tetragonal space group $P4_12_12$ with one molecule (half a dimer) in the crystallographic asymmetric unit. Data were processed by XDS [52] and CCP4 [53], and the structure was solved by Phaser [48], which is reported here. The resulting model was improved by iterative rounds of refinement and model building using REFMAC5 and O [54,55]. Water molecules were added to the atomic model automatically using ARP-w-ARP [56] at the positions of large positive peaks in the difference electron density, but only at places where the resulting water molecule fell into an appropriate hydrogen bonding environment. Data processing and refinement statistics are given in Table 4. The final model contains residues 21–723, and was visualised in, and figures produced using, PyMol [57].

The PDB ID is 5OLJ.

5.5. Modelling and docking

The crystal structures of many human DPP4 (hDPP4) proteins, co-crystallized with substrate analogues or other types of

Table 4
Summary of crystallographic data collection and refinement statistics.

Data collection	
Radiation, detector and wavelength (Å)	CuKα, MAR345, 1.5418
Unit cell (Å)	a = b = 109.10, c = 157.81
Space group	$P4_12_12$
Resolution (Å)	38–2.2 (2.32–2.2)
Observations	453,350
Unique reflections	48,811
I/σ(I)	10.8 (3.3)
R_{sym}[a]	0.424 (0.971)
Completeness (%)	99.7 (96.6)
$CC_{1/2}$[b]	0.992 (0.973)
Refinement	
Non-hydrogen atoms	6034 (including 1 glycerol & 396 waters)
R_{cryst}[c]	0.224 (0.529)
Reflections used	46,837 (3288)
R_{free}[d]	0.254 (0.531)
Reflections used	1974 (137)
R_{cryst} (all data)[b]	0.225
Average temperature factors (Å^2)	
All atoms	16.7
Protein	16.6
Glycerol	31.2
Water	16.2
Rmsds from ideal values	
Bonds (Å)	0.014
Angles (°)	1.6
DPI coordinate error (Å)[e]	0.18
Ramachandran Plot (%)	
Most favoured	96.1
Additional allowed	3.6
Outliers	0.3
wwPDB code	5OLJ

Numbers in parentheses refer to values in the highest resolution shell.

[a] $R_{sym} = \Sigma_j\Sigma_h|I_{h,j} - \langle I_h\rangle|/\Sigma_j\Sigma_h\langle I_h\rangle$ where $I_{h,j}$ is the jth observation of reflection h, and $\langle I_h\rangle$ is the mean intensity of that reflection.

[b] $CC_{1/2}$ is the correlation coefficient of the mean intensities between two random half-sets of data.

[c] $R_{cryst} = \Sigma||F_{obs}|-|F_{calc}||/\Sigma|F_{obs}|$ where F_{obs} and F_{calc} are the observed and calculated structure factor amplitudes, respectively.

[d] R_{free} is equivalent to R_{cryst} for a 4% subset of reflections not used in the refinement.

[e] DPI refers to the diffraction component precision index [62].

inhibitors, were taken from the PDB. The structures used are listed in supplementary material Table S1. The coordinates of the catalytic triad residues from each of these human DPP4s were structurally aligned onto the corresponding pgDPP4 coordinates and the derived transformation matrices were subsequently applied to each of the co-crystallized ligands.

Acknowledgements

Initial crystallographic data were collected at beam lines ID44-4, ESRF, France, and we acknowledge the support of the beam line scientists. We thank Dr Yumi Kumagai for providing the pgDPP4 DNA.

This project was supported by the Fund for Scientific Research (FWO-Flanders, Belgium, Project code G.0173.09N) to AML and PVDV; the Agency for Innovation by Science and Technology in Flanders (IWT, Belgium, grant SBO 50164 “Functional peptidomics”) to BL, LS and WL; the IOF/KP/09/003 “functional peptidomics platform” of the Industrial Research Fund of the University of Leuven to BL, LS and WL; and EU-FP7 HEALTH-Proposal No. 223077 (NEUROPRO) to VF, DR and AML. BL is an IOF fellow. We thank W.L. for the time he donated to this project at his own expense.

Appendix A. Supplementary data

Supplementary data related to this article can be found at http://dx.doi.org/10.1016/j.ejmech.2017.08.024.

References

[1] N. Bostanci, G.N. Belibasakis, *Porphyromonas gingivalis*: an invasive and evasive opportunistic oral pathogen, FEMS Microbiol. Lett. 333 (2012) 1–9.
[2] S.J. Byrne, S.G. Dashper, I.B. Darby, G.G. Adams, B. Hoffmann, E.C. Reynolds, Progression of chronic periodontitis can be predicted by the levels of *Porphyromonas gingivalis* and *Treponema denticola* in subgingival plaque, Oral Microbiol. Immunol. 24 (2009) 469–477.
[3] A. Holmlund, M. Hedin, P.J. Pussinen, U.H. Lerner, L. Lind, *Porphyromonas gingivalis* (Pg) a possible link between impaired oral health and acute myocardial infarction, Int. J. Cardiol. 148 (2011) 148–153.
[4] S. Offenbacher, K.A. Boggess, A.P. Murtha, H.L. Jared, S. Lieff, R.G. McKaig, S.M. Mauriello, K.L. Moss, J.D. Beck, Progressive periodontal disease and risk of very preterm delivery, Obstet. Gynecol. 107 (2006) 29–36.
[5] F.A. Scannapieco, Pneumonia in nonambulatory patients. The role of oral bacteria and oral hygiene, J. Am. Dent. Assoc. (137 Suppl) (2006) 21S–25S.
[6] G. Hajishengallis, *Porphyromonas gingivalis*-host interactions: open war or intelligent guerilla tactics? Microbes Infect. 11 (2009) 637–645.
[7] O. Yilmaz, The chronicles of *Porphyromonas gingivalis*: the microbium, the human oral epithelium and their interplay, Microbiology 154 (2008) 2897–2903.
[8] H. Oda, K. Saiki, Y. Numabe, K. Konishi, Effect of gamma-immunoglobulin on the asaccharolytic growth of *Porphyromonas gingivalis*, J. Periodontal Res. 42 (2007) 438–442.
[9] H. Oda, K. Saiki, M. Tonosaki, A. Yajima, K. Konishi, Participation of the secreted dipeptidyl and tripeptidyl aminopeptidases in asaccharolytic growth of *Porphyromonas gingivalis*, J. Periodontal Res. 44 (2009) 362–367.
[10] J. Potempa, R.N. Pike, Corruption of innate immunity by bacterial proteases, J. Innate Immun. 1 (2009) 70–87.
[11] Y. Kumagai, K. Konishi, T. Gomi, H. Yagishita, A. Yajima, M. Yoshikawa, Enzymatic properties of dipeptidyl aminopeptidase IV produced by the periodontal pathogen *Porphyromonas gingivalis* and its participation in virulence, Infect. Immun. 68 (2000) 716–724.
[12] A. Banbula, M. Bugno, J. Goldstein, J. Yen, D. Nelson, J. Travis, J. Potempa, Emerging family of proline-specific peptidases of *Porphyromonas gingivalis*: purification and characterization of serine dipeptidyl peptidase, a structural and functional homologue of mammalian prolyl dipeptidyl peptidase IV, Infect. Immun. 68 (2000) 1176–1182.
[13] Y. Kumagai, H. Yagishita, A. Yajima, T. Okamoto, K. Konishi, Molecular mechanism for connective tissue destruction by dipeptidyl aminopeptidase IV produced by the periodontal pathogen *Porphyromonas gingivalis*, Infect. Immun. 73 (2005) 2655–2664.
[14] H. Yagishita, Y. Kumagai, K. Konishi, Y. Takahashi, T. Aoba, M. Yoshikawa, Histopathological studies on virulence of dipeptidyl aminopeptidase IV (DPPIV) of *Porphyromonas gingivalis* in a mouse abscess model: use of a DPPIV-deficient mutant, Infect. Immun. 69 (2001) 7159–7161.
[15] Y. Kumagai, A. Yajima, K. Konishi, Peptidase activity of dipeptidyl aminopeptidase IV produced by *Porphyromonas gingivalis* is important but not sufficient for virulence, Microbiol. Immunol. 47 (2003) 735–743.
[16] S. Clais, G. Boulet, M. Kerstens, T. Horemans, W. Teughels, M. Quirynen, E. Lanckacker, I. De Meester, A.M. Lambeir, P. Delputte, L. Maes, P. Cos, Importance of biofilm formation and dipeptidyl peptidase IV for the pathogenicity of clinical *Porphyromonas gingivalis* isolates, Pathog. Dis. 70 (2014) 408–413.
[17] A.M. Lambeir, D. Rea, V. Fulop, Y. Kumagai, K. Augustyns, I. de Meester, A. Haemers, S. Scharpe, Exploration of the active site of dipeptidyl peptidase IV from *Porphyromonas gingivalis*. Comparison with the human enzyme, Adv. Exp. Med. Biol. 524 (2003) 29–35.
[18] D. Rea, A.M. Lambeir, Y. Kumagai, I. De Meester, S. Scharpe, V. Fulop, Expression, purification and preliminary crystallographic analysis of dipeptidyl peptidase IV from *Porphyromonas gingivalis*, Acta Crystallogr. D. Biol. Crystallogr. 60 (2004) 1871–1873.
[19] M. Nauck, Incretin therapies: highlighting common features and differences in the modes of action of glucagon-like peptide-1 receptor agonists and dipeptidyl peptidase-4 inhibitors, Diabetes Obes. Metab. 18 (2016) 203–216.
[20] A. Belyaev, X. Zhang, K. Augustyns, A.M. Lambeir, I. De Meester, I. Vedernikova, S. Scharpe, A. Haemers, Structure-activity relationship of diaryl phosphonate esters as potent irreversible dipeptidyl peptidase IV inhibitors, J. Med. Chem. 42 (1999) 1041–1052.
[21] L. Heirbaut, S. van Goethem, K. Jansen, H. de Winter, N. Lamoen, J. Joossens, J. Cheng, X. Chen, A.M. Lambeir, I. de Meester, K. Augustyns, P. van der Veken, Probing for improved selectivity with dipeptide-derived inhibitors of dipeptidyl peptidases 8 and 9: the impact of P1-variation, MedChemComm 7 (2016) 433–438.
[22] K. Jansen, L. Heirbaut, J.D. Cheng, J. Joossens, O. Ryabtsova, P. Cos, L. Maes, A.M. Lambeir, I. De Meester, K. Augustyns, P. Van der Veken, Selective inhibitors of fibroblast activation protein (FAP) with a (4-Quinolinoyl)-glycyl-2-cyanopyrrolidine scaffold, ACS Med. Chem. Lett. 4 (2013) 491–496.
[23] K. Jansen, L. Heirbaut, R. Verkerk, J.D. Cheng, J. Joossens, P. Cos, L. Maes, A.M. Lambeir, I. De Meester, K. Augustyns, P. Van der Veken, Extended structure-activity relationship and pharmacokinetic investigation of (4-quinolinoyl)glycyl-2-cyanopyrrolidine inhibitors of fibroblast activation protein (FAP), J. Med. Chem. 57 (2014) 3053–3074.
[24] A.M. Lambeir, M. Borloo, I. De Meester, A. Belyaev, K. Augustyns, D. Hendriks, S. Scharpe, A. Haemers, Dipeptide-derived diphenyl phosphonate esters: mechanism-based inhibitors of dipeptidyl peptidase IV, Biochim. Biophys. Acta 1290 (1996) 76–82.
[25] O. Ryabtsova, K. Jansen, S. Van Goethem, J. Joossens, J.D. Cheng, A.M. Lambeir, I. De Meester, K. Augustyns, P. Van der Veken, Acylated Gly-(2-cyano)pyrrolidines as inhibitors of fibroblast activation protein (FAP) and the issue of FAP/prolyl oligopeptidase (PREP)-selectivity, Bioorg Med. Chem. Lett. 22 (2012) 3412–3417.
[26] K. Senten, P. Van der Veken, G. Bal, I. De Meester, A.M. Lambeir, S. Scharpe, B. Bauvois, A. Haemers, K. Augustyns, Development of potent and selective dipeptidyl peptidase II inhibitors, Bioorg Med. Chem. Lett. 12 (2002) 2825–2828.
[27] K. Senten, P. Van Der Veken, I. De Meester, A.M. Lambeir, S. Scharpe, A. Haemers, K. Augustyns, Gamma-amino-substituted analogues of 1-[(S)-2,4-diaminobutanoyl]piperidine as highly potent and selective dipeptidyl peptidase II inhibitors, J. Med. Chem. 47 (2004) 2906–2916.
[28] A. Soroka, P. Van der Veken, I. De Meester, A.M. Lambeir, M.B. Maes, S. Scharpe, A. Haemers, K. Augustyns, Synthesis and dipeptidyl peptidase inhibition of N-(4-substituted-2,4-diaminobutanoyl)piperidines, Bioorg Med. Chem. Lett. 16 (2006) 4777–4779.
[29] P. Van der Veken, I. De Meester, V. Dubois, A. Soroka, S. Van Goethem, M.B. Maes, I. Brandt, A.M. Lambeir, X. Chen, A. Haemers, S. Scharpe, K. Augustyns, Inhibitors of dipeptidyl peptidase 8 and dipeptidyl peptidase 9. Part 1: identification of dipeptide derived leads, Bioorg Med. Chem. Lett. 18 (2008) 4154–4158.
[30] P. Van der Veken, V. Fulop, D. Rea, M. Gerard, R. Van Elzen, J. Joossens, J.D. Cheng, V. Baekelandt, I. De Meester, A.M. Lambeir, K. Augustyns, P2-substituted N-acylprolylpyrrolidine inhibitors of prolyl oligopeptidase: biochemical evaluation, binding mode determination, and assessment in a cellular model of synucleinopathy, J. Med. Chem. 55 (2012) 9856–9867.
[31] P. Van der Veken, A. Soroka, I. Brandt, Y.S. Chen, M.B. Maes, A.M. Lambeir, X. Chen, A. Haemers, S. Scharpe, K. Augustyns, I. De Meester, Irreversible inhibition of dipeptidyl peptidase 8 by dipeptide-derived diaryl phosphonates, J. Med. Chem. 50 (2007) 5568–5570.
[32] S. Van Goethem, V. Matheeussen, J. Joossens, A.M. Lambeir, X. Chen, I. De Meester, A. Haemers, K. Augustyns, P. Van der Veken, Structure-activity relationship studies on isoindoline inhibitors of dipeptidyl peptidases 8 and 9 (DPP8, DPP9): is DPP8-selectivity an attainable goal? J. Med. Chem. 54 (2011) 5737–5746.
[33] S. Van Goethem, P. Van der Veken, V. Dubois, A. Soroka, A.M. Lambeir, X. Chen, A. Haemers, S. Scharpe, I. De Meester, K. Augustyns, Inhibitors of dipeptidyl peptidase 8 and dipeptidyl peptidase 9. Part 2: isoindoline containing inhibitors, Bioorg Med. Chem. Lett. 18 (2008) 4159–4162.
[34] H.B. Rasmussen, S. Branner, F.C. Wiberg, N. Wagtmann, Crystal structure of human dipeptidyl peptidase IV/CD26 in complex with a substrate analog, Nat. Struct. Biol. 10 (2003) 19–25.
[35] M. Nabeno, F. Akahoshi, H. Kishida, I. Miyaguchi, Y. Tanaka, S. Ishii, T. Kadowaki, A comparative study of the binding modes of recently launched

dipeptidyl peptidase IV inhibitors in the active site, Biochem. Biophys. Res. Commun. 434 (2013) 191–196.
[36] W.J. Metzler, J. Yanchunas, C. Weigelt, K. Kish, H.E. Klei, D. Xie, Y. Zhang, M. Corbett, J.K. Tamura, B. He, L.G. Hamann, M.S. Kirby, J. Marcinkeviciene, Involvement of DPP-IV catalytic residues in enzyme-saxagliptin complex formation, Protein Sci. 17 (2008) 240–250.
[37] J. Li, E. Wilk, S. Wilk, Aminoacylpyrrolidine-2-nitriles: potent and stable inhibitors of dipeptidyl-peptidase IV (CD 26), Arch. Biochem. Biophys. 323 (1995) 148–154.
[38] I. Brandt, J. Joossens, X. Chen, M.B. Maes, S. Scharpe, I. De Meester, A.M. Lambeir, Inhibition of dipeptidyl-peptidase IV catalyzed peptide truncation by Vildagliptin ((2S)-{[(3-hydroxyadamantan-1-yl)amino]acetyl}-pyrrolidine-2-carbonitrile), Biochem. Pharmacol. 70 (2005) 134–143.
[39] R. Van Elzen, E. Schoenmakers, I. Brandt, P. Van Der Veken, A.M. Lambeir, Ligand-induced conformational changes in prolyl oligopeptidase: a kinetic approach, Protein Eng. Des. Sel. 30 (2017) 8.
[40] C. Rummey, G. Metz, Homology models of dipeptidyl peptidases 8 and 9 with a focus on loop predictions near the active site, Proteins 66 (2007) 160–171.
[41] V. Matheeussen, Y. Waumans, W. Martinet, S. Van Goethem, P. Van der Veken, S. Scharpe, K. Augustyns, G.R. De Meyer, I. De Meester, Dipeptidyl peptidases in atherosclerosis: expression and role in macrophage differentiation, activation and apoptosis, Basic Res. Cardiol. 108 (2013) 350.
[42] Y. Waumans, G. Vliegen, L. Maes, M. Rombouts, K. Declerck, P. Van Der Veken, W. Vanden Berghe, G.R. De Meyer, D. Schrijvers, I. De Meester, The dipeptidyl peptidases 4, 8, and 9 in mouse monocytes and macrophages: DPP8/9 inhibition attenuates M1 macrophage activation in mice, Inflammation 39 (2016) 413–424.
[43] Y. Nakajima, K. Ito, T. Toshima, T. Egawa, H. Zheng, H. Oyama, Y.F. Wu, E. Takahashi, K. Kyono, T. Yoshimoto, Dipeptidyl aminopeptidase IV from *Stenotrophomonas maltophilia* exhibits activity against a substrate containing a 4-hydroxyproline residue, J. Bacteriol. 190 (2008) 7819–7829.
[44] S. Kaushik, R. Sowdhamini, Distribution, classification, domain architectures and evolution of prolyl oligopeptidases in prokaryotic lineages, BMC Genomics 15 (2014) 985.
[45] K. Boonen, S.J. Husson, B. Landuyt, G. Baggerman, E. Hayakawa, W.H. Luyten, L. Schoofs, Identification and relative quantification of neuropeptides from the endocrine tissues, Methods Mol. Biol. 615 (2010) 191–206.
[46] E. Clynen, F. Liu, S.J. Husson, B. Landuyt, E. Hayakawa, G. Baggerman, G. Wets, L. Schoofs, Bioinformatic approaches to the identification of novel neuropeptide precursors, Methods Mol. Biol. 615 (2010) 357–374.
[47] Z. Otwinowski, W. Minor, [20] Processing of X-ray diffraction data collected in oscillation mode, Methods Enzymol. 276 (1997) 307–326.
[48] A.J. McCoy, R.W. Grosse-Kunstleve, P.D. Adams, M.D. Winn, L.C. Storoni, R.J. Read, Phaser crystallographic software, J. Appl. Crystallogr. 40 (2007) 658–674.
[49] T. Terwilliger, SOLVE and RESOLVE: automated structure solution, density modification and model building, J. Synchrotron Radiat. 11 (2004) 49–52.
[50] K. Cowtan, The Buccaneer software for automated model building. 1. Tracing protein chains, Acta Crystallogr. D. Biol. Crystallogr. 62 (2006) 1002–1011.
[51] F. Gorrec, The MORPHEUS protein crystallization screen, J. Appl. Crystallogr. 42 (2009) 1035–1042.
[52] W. Kabsch, Xds, Acta Crystallogr. D. Biol. Crystallogr. 66 (2010) 125–132.
[53] N. Collaborative Computational Project, The CCP4 suite: programs for protein crystallography, Acta Crystallogr. D. Biol. Crystallogr. 50 (1994) 760–763.
[54] T.A. Jones, J.Y. Zou, S.W. Cowan, M. Kjeldgaard, Improved methods for building protein models in electron density maps and the location of errors in these models, Acta Crystallogr. A 47 (Pt 2) (1991) 110–119.
[55] G.N. Murshudov, P. Skubak, A.A. Lebedev, N.S. Pannu, R.A. Steiner, R.A. Nicholls, M.D. Winn, F. Long, A.A. Vagin, REFMAC5 for the refinement of macromolecular crystal structures, Acta Crystallogr. D. Biol. Crystallogr. 67 (2011) 355–367.
[56] A. Perrakis, R. Morris, V.S. Lamzin, Automated protein model building combined with iterative structure refinement, Nat. Struct. Biol. 6 (1999) 458–463.
[57] W.L. DeLano, The PyMOL user's manual, in: DeLano Scientific, Palo Alto, CA, 2002.
[58] S.E. Poplawski, J.H. Lai, Y. Li, Z. Jin, Y. Liu, W. Wu, Y. Wu, Y. Zhou, J.L. Sudmeier, D.G. Sanford, W.W. Bachovchin, Identification of selective and potent inhibitors of fibroblast activation protein and prolyl oligopeptidase, J. Med. Chem. 56 (2013) 3467–3477.
[59] D. Kim, L. Wang, M. Beconi, G.J. Eiermann, M.H. Fisher, H. He, G.J. Hickey, J.E. Kowalchick, B. Leiting, K. Lyons, F. Marsilio, M.E. McCann, R.A. Patel, A. Petrov, G. Scapin, S.B. Patel, R.S. Roy, J.K. Wu, M.J. Wyvratt, B.B. Zhang, L. Zhu, N.A. Thornberry, A.E. Weber, (2R)-4-oxo-4-[3-(trifluoromethyl)-5,6-dihydro[1,2,4]triazolo[4,3-a]pyrazin-7(8H)- yl]-1-(2,4,5-trifluorophenyl) butan-2-amine: a potent, orally active dipeptidyl peptidase IV inhibitor for the treatment of type 2 diabetes, J. Med. Chem. 48 (2005) 141–151.
[60] G.R. Lankas, B. Leiting, R.S. Roy, G.J. Eiermann, M.G. Beconi, T. Biftu, C.C. Chan, S. Edmondson, W.P. Feeney, H. He, D.E. Ippolito, D. Kim, K.A. Lyons, H.O. Ok, R.A. Patel, A.N. Petrov, K.A. Pryor, X. Qian, L. Reigle, A. Woods, J.K. Wu, D. Zaller, X. Zhang, L. Zhu, A.E. Weber, N.A. Thornberry, Dipeptidyl peptidase IV inhibition for the treatment of type 2 diabetes: potential importance of selectivity over dipeptidyl peptidases 8 and 9, Diabetes 54 (2005) 2988–2994.
[61] M. Eckhardt, E. Langkopf, M. Mark, M. Tadayyon, L. Thomas, H. Nar, W. Pfrengle, B. Guth, R. Lotz, P. Sieger, H. Fuchs, F. Himmelsbach, 8-(3-(R)-aminopiperidin-1-yl)-7-but-2-ynyl-3-methyl-1-(4-methyl-quinazolin-2-ylmethyl)-3,7-dihydropurine-2,6-dione (BI 1356), a highly potent, selective, long-acting, and orally bioavailable DPP-4 inhibitor for the treatment of type 2 diabetes, J. Med. Chem. 50 (2007) 6450–6453.
[62] D.W. Cruickshank, Remarks about protein structure precision, Acta Crystallogr. D. Biol. Crystallogr. 55 (1999) 583–601.
[63] C.E. Grimshaw, A. Jennings, R. Kamran, H. Ueno, N. Nishigaki, T. Kosaka, A. Tani, H. Sano, Y. Kinugawa, E. Koumura, L. Shi, K. Takeuchi, Trelagliptin (SYR-472, Zafatek), novel once-weekly treatment for type 2 diabetes, inhibits dipeptidyl Peptidase-4 (DPP-4) via a non-covalent mechanism, PLoS One 11 (2016) e0157509.
[64] R.J. Read, Improved Fourier coefficients for maps using phases from partial structures with errors, Acta Crystallogr. A Found. Adv. 42 (1986) 140–149.
[65] S.D. Edmondson, A. Mastracchio, R.J. Mathvink, J. He, B. Harper, Y.J. Park, M. Beconi, J. Di Salvo, G.J. Eiermann, H. He, B. Leiting, J.F. Leone, D.A. Levorse, K. Lyons, R.A. Patel, S.B. Patel, A. Petrov, G. Scapin, J. Shang, R.S. Roy, A. Smith, J.K. Wu, S. Xu, B. Zhu, N.A. Thornberry, A.E. Weber, (2S,3S)-3-Amino-4-(3,3-difluoropyrrolidin-1-yl)-N,N-dimethyl-4-oxo-2-(4-[1,2,4]tr iazolo[1,5-a]-pyridin-6-ylphenyl)butanamide: a selective alpha-amino amide dipeptidyl peptidase IV inhibitor for the treatment of type 2 diabetes, J. Med. Chem. 49 (2006) 3614–3627.